Evidence of Incoherent Carriers Associated with Resonant Impurity Levels and Their Influence on Superconductivity in the Anomalous Superconductor $Pb_{1-x}Tl_xTe$

P. Giraldo-Gallo,[1,2,3] P. Walmsley,[4] B. Sangiorgio,[5] S. C. Riggs,[2] R. D. McDonald,[6] L. Buchauer,[7] B. Fauqué,[7] Chang Liu,[8] N. A. Spaldin,[5] A. Kaminski,[8] K. Behnia,[7] and I. R. Fisher[4]

[1]*Geballe Laboratory for Advanced Materials and Department of Physics, Stanford University, Stanford, California 94305, USA*

[2]*National High Magnetic Field Laboratory, Tallahassee, Florida 32310, USA*

[3]*Department of Physics, Universidad de Los Andes, Bogotá 111711, Colombia*

[4]*Geballe Laboratory for Advanced Materials and Department of Applied Physics, Stanford University, Stanford, California 94305, USA*

[5]*Materials Theory, ETH Zurich, Wolfgang-Pauli-Strasse 27, CH-8093 Zürich, Switzerland*

[6]*Los Alamos National Laboratory, Los Alamos, New Mexico 87545, USA*

[7]*LPEM (UPMC-CNRS), Ecole Superieure de Physique et de Chimie Industrielles, Rue Vauquelin, 75005 Paris, France*

[8]*Ames Laboratory and Department of Physics and Astronomy, Iowa State University, Ames, Iowa 50011, USA*

(Received 15 November 2017; published 13 November 2018)

We present a combined experimental and theoretical study of the evolution of the Fermi surface of the anomalous superconductor $Pb_{1-x}Tl_xTe$ as a function of thallium concentration, drawing on a combination of magnetotransport measurements (Shubnikov–de Haas oscillations and the Hall coefficient), angle resolved photoemission spectroscopy, and density functional theory calculations of the electronic structure. Our results indicate that for Tl concentrations beyond a critical value, the Fermi energy coincides with resonant impurity states in $Pb_{1-x}Tl_xTe$, and we rule out the presence of an additional valence band maximum at the Fermi energy. A comparison to nonsuperconducting $Pb_{1-x}Na_xTe$ implies that the presence of these impurity states at the Fermi energy provides the enhanced pairing interaction and thus also the anomalously high temperature superconductivity in this material.

DOI: 10.1103/PhysRevLett.121.207001

$Pb_{1-x}Tl_xTe$ is a hole-doped narrow band-gap semiconductor that exhibits, by far, the highest known superconducting critical temperature, T_c, of any material of equivalent carrier density [1,2]. Superconductivity in very low density systems is in itself unexpected from the conventional phonon-mediated BCS theory of superconductivity, and it has prompted the discussion of a number of exotic pairing mechanisms. In n-doped $SrTiO_3$, for example, nonadiabatic phonon pairing [3,4], pairing through the exchange of a plasmonic [5] or a soft optical phonon mode [6], pairing from quantum ferroelectric fluctuations [7], and an enhancement of the density of states (DOS) and/or pairing potential due to multiband Fermi surface (FS) effects [8–10] have been proposed; whereas enhanced electronic correlations from multivalley FS effects have been invoked to explain the recently discovered bulk superconductivity in Bismuth [11,12]. The present case of superconductivity in PbTe, however, has the additional curiosity of occurring only when hole doping is achieved by thallium (Tl) impurities [13,14], which suggests that a unique property of the dopant may be key.

A number of experimental studies have inferred the presence of shallow impurity levels in the valence band of $Pb_{1-x}Tl_xTe$ [13]. Density functional theory (DFT) calculations [15,37,38] find that low levels of atomic substitution profoundly modify the band structure. Therefore, doping cannot be pictured as a rigid shift of the chemical potential. In the case of Tl, the valence of impurity states depend on the position of Fermi energy, E_F. For large (small) hole concentrations, Tl^{3+} (Tl^{1+}) is favored [38]. Interestingly, these distinct charge states become energetically degenerate when E_F lies about 50 meV below the top of the valence band, as suggested by earlier heuristic arguments [13]. Charge fluctuations associated with such resonant impurity states have been proposed as an alternative pairing interaction in Tl-doped PbTe [39–41], potentially accounting for the anomalously high T_c and other normal state properties [42,43], and possibly related to similar ideas suggested for doped $BaBiO_3$ [44–46]. However, other scenarios are also possible, in particular a second (heavy) valence band maximum occurs at a similar energy in DFT calculations [47], raising the alternative view that additional pockets

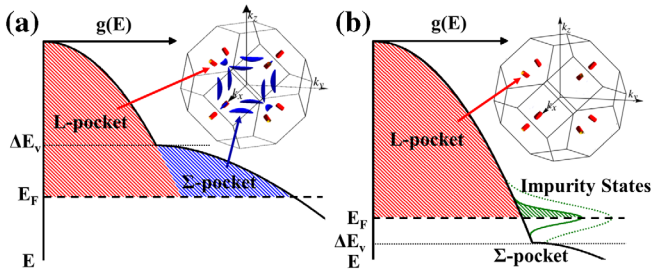

FIG. 1. Illustration of two possible scenarios of valence band filling in $Pb_{1-x}Tl_xTe$, showing schematic diagrams of the DOS $g(E)$ as a function of energy E, and the FS morphology (insets). (a) The situation in which $E_F > \Delta E_v$ and the impurity states play no role. The upper valence band maximum (the L-pocket, red) and the second valence band maximum (the Σ-pocket, blue) are both above E_F, giving four degenerate valleys for L-states and twelve degenerate valleys for Σ-states, and an increased DOS for $E_F > \Delta E_v$, where ΔE_v is the difference in energy between the band maxima. Inset: Calculated FS for $E_F > \Delta E_v$ [47]. (b) The situation in which the Σ-band is never populated because resonant impurity states (shown in green) associated with Tl doping occur at $E = E_F < \Delta E_v$. E_F is pinned by resonant impurity states at an energy $E_F < \Delta E_v$, leading to an increase in the DOS. Inset: Calculated FS for $E_F < \Delta E_v$ [47]. In this Letter, we establish that scenario (b) is the correct description for $Pb_{1-x}Tl_xTe$ with $x > x_c$, with immediate implications for the origin of the anomalous superconductivity observed for this material.

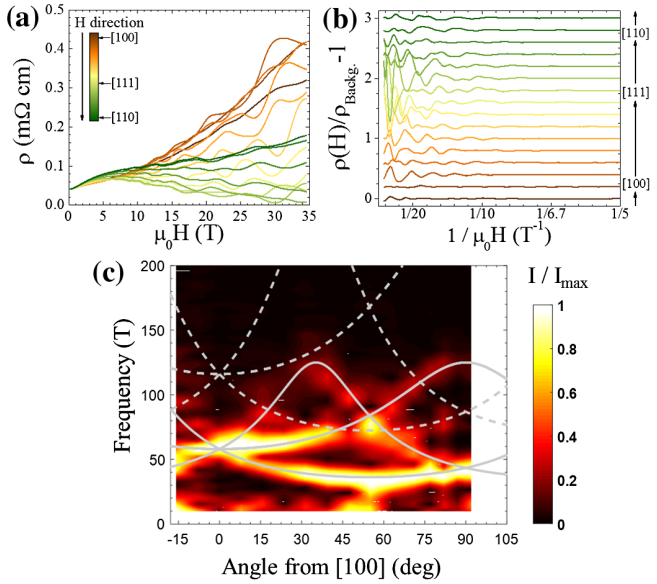

FIG. 2. Magnetoresistance measurements as a function of magnetic field rotated in the (110) plane for a representative sample $Pb_{1-x}Tl_xTe$ with $x = 0.15\%$. (a) Symmetrized resistivity, $[\rho_{xx}(H) + \rho_{xx}(-H)]/2$, as a function of the applied magnetic field for different field orientations along the (110) plane. (b) The oscillating component of the corresponding magnetoresistance curves in (a) as a function of inverse field. (c) Amplitude of the normalized FFT, represented by the color scale, as a function of the angle of the field from the [100] direction, and the frequency. The white curves are the expected angular evolution for a perfect ellipsoidal model (solid-lines for fundamental frequencies, dashed-lines for second-harmonics).

in the FS could produce a less exotic superconducting mechanism by increasing the DOS and/or providing additional interband scattering mechanisms [14]. These two scenarios, illustrated in Fig. 1, can be distinguished based on the characterization of the low-energy electronic structure of Tl-doped PbTe. Here, we present a combined experimental and computational study of the low-energy electronic structure and FS of $Pb_{1-x}Tl_xTe$, utilizing Shubnikov–de Haas (SdH), angle resolved photoemission spectroscopy (ARPES), and Hall effect measurements, as well as DFT calculations of the electronic structure [15]. We definitively establish that the Σ-pocket remains well below E_F for all compositions of $Pb_{1-x}Tl_xTe$, and therefore, it does not drive the superconductivity in this material. Furthermore, by contrasting our data with similar data from the nonsuperconducting analog $Pb_{1-x}Na_xTe$, we observe a number of phenomena that distinguish superconducting and nonsuperconducting compositions, which we show to be consistent with the presence of additional mobile charges associated with the resonant impurity states introduced by Tl doping.

Single crystals of $Pb_{1-x}Tl_xTe$ were grown by an unseeded physical vapor transport method [15]. For magnetoresistance measurements, the crystals were cleaved into [100] oriented rectilinear bars. Electrical contacts were made in a 4-point geometry. Compositions of $x = 0\%$, 0.15%, and 0.4% were measured to 35 T at the DC facility of the National High Magnetic Field Laboratory (NHMFL) in Tallahassee, FL, USA; $x = 0.3\%$, 0.8%, and 1.3% were measured to 32 T (DC) at the High Field Magnet Laboratory in Nijmegen, The Netherlands; and additional measurements for $x = 0.15\%$ and 0.8% were taken up to 60 T at the pulsed field facility of the NHMFL, in Los Alamos National Laboratory. The angle dependent data were obtained at a temperature of (1.5 ± 0.2) K using a single-axis rotator probe. Hall measurements were taken for all of the samples studied at a temperature of 1.5 K. ARPES measurements were performed at the beam line 7.0.1 of the Advanced Light Source and at the Surface and Interface Spectroscopy beam line of the Swiss Light Source, Switzerland, using a photon energy of $h\nu = 70$ eV at 40 K. All samples were cleaved *in situ* prior to measurement.

Figure 2(a) shows the magnetoresistance of a representative $Pb_{1-x}Tl_xTe$ sample with $x = 0.15\%$ (with Hall number $p_H = 1.67 \times 10^{19}\text{cm}^{-3}$) for different field orientations in the (110) plane, clearly exhibiting SdH oscillations. The (110) plane is a natural plane to study the angle evolution of the SdH frequencies in PbTe as it passes through all of the crystallographic high symmetry directions and allows the determination of both the transverse and longitudinal extremal cross-sectional areas of the ellipsoidal pocket, known to describe the first valence

band maximum situated at the L-point (the "L-pocket") in PbTe. Figure 2(b) shows the oscillating component of the magnetoresistance as a function of the inverse field, where the nonoscillating component has been removed by fitting and subtracting a cubic spline from the data in Fig. 2(a). Fourier analysis reveals multiple oscillatory components that are periodic in the inverse field, as expected for quantum oscillations, with frequencies and magnitudes that vary as a function of the angle. This variation is illustrated in Fig. 2(c), which shows how the amplitude of the fast Fourier transformation (FFT) of the oscillatory component of the magnetoresistance [Fig. 2(b)] evolves with frequency and angle. Similarly to the nonsuperconducting Na-doped analog [47], all of the frequencies observed at every angle can be very well fitted by fundamental and second harmonics corresponding to four ellipsoidal FS pockets at the L-point. This analysis was repeated for each sample [15] and yields the values of the minimum and maximum cross sectional areas of the L-pocket, which for this particular composition are $f_{\mathrm{min}} = (36 \pm 9)$ T and $f_{\mathrm{max}} = (125 \pm 8)$ T, respectively. No signature of the Σ-pocket or any features of nonellipsoidicity of the L-pocket were observed at any composition measured in this study.

The values of f_{min}, f_{max}, and $f_{[100]}$ (SdH frequency with $B\|[100]$), of the L-pocket measured here in $Pb_{1-x}Tl_xTe$ are shown in Figs. 3(b)–3(d) as a function of Hall number p_H (which is a good approximation to carrier concentration in a single band-ellipsoidal FS [47,48]), and compared to the same values previously found in nonsuperconducting $Pb_{1-x}Na_xTe$ [47] and $Pb_{1-\delta}Te$ [49,50]. As discussed in Ref. [47], in $Pb_{1-x}Na_xTe$ and $Pb_{1-\delta}Te$ the cross sectional areas follow the $p_H^{2/3}$ evolution expected for a single-band perfect ellipsoidal model for the entire range of carrier concentration (except for the highest Na doping measured, where there may be a small deviation). This model also holds for nonsuperconducting concentrations of Tl where $x < x_c$, but there is a clear break from this trend for $x > x_c$ in $Pb_{1-x}Tl_xTe$ with the deviation growing as x increases concurrently with T_c [see Fig. 3(a)]. Evidently, the emergence of superconductivity in $Pb_{1-x}Tl_xTe$ is concomitant with the formation of a second electronic reservoir distinct from the L-pockets.

In nonsuperconducting $Pb_{1-x}Na_xTe$, the Luttinger volume of the L-pocket and p_H are in excellent agreement for all compositions, indicating that all mobile charges are contained within the L-pocket [47]. This is shown in Fig. 4(a), where the black line shows the expectation if each dopant contributes a single carrier (or equivalently two carriers per lead vacancy), and the Luttinger volume of $Pb_{1-x}Na_xTe$ (black squares) follows this closely. However, the present data show that $Pb_{1-x}Tl_xTe$ departs from this trend for $x > x_c$. The Hall number (open red circles) falls below the expected value if each Tl dopant were to contribute a single hole (as expected for a Tl^{1+} valence), but it still gives a significantly

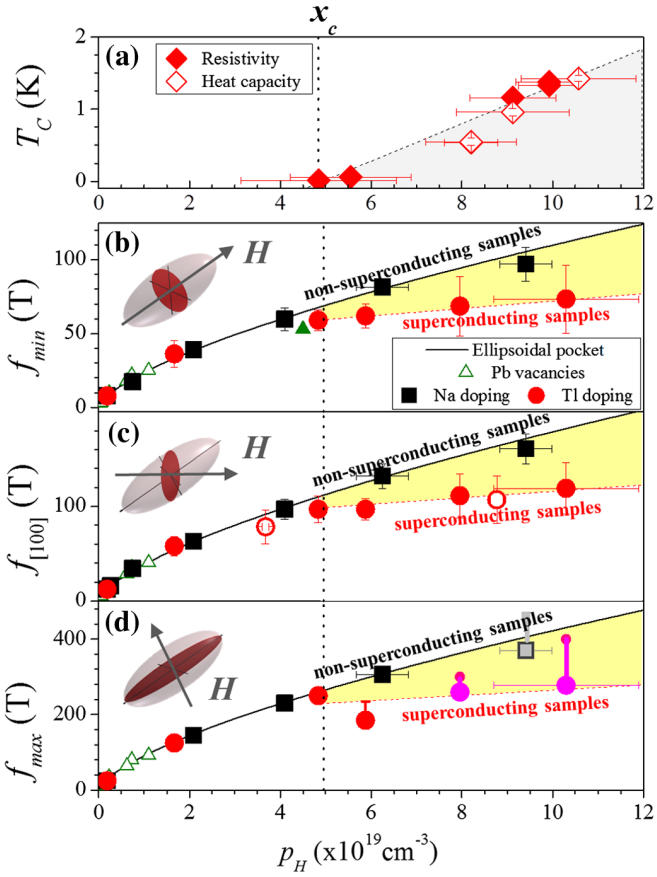

FIG. 3. Comparison of T_c {panel (a); from Ref. [43]} and L-pocket cross-sectional areas [panels (b)–(d)] as a function of the measured Hall number, of Tl-doped PbTe (red data points), nonsuperconducting Na-doped PbTe (black data points, from Ref. [47]; and solid-green data point from Ref. [49]), and nonsuperconducting $Pb_{1-\delta}Te$ (open-green data points, from Refs. [49,50]. Insets illustrate the field orientations relative to the L-pocket (pink ellipse), corresponding to angles of 54.7°, 0°, and 35.3° relative to [100]. The difference between superconducting and nonsuperconducting compositions is highlighted by yellow shading. Solid black lines in panels (b)–(d) illustrate the functional dependence of $p_H^{2/3}$ expected for a perfect ellipsoidal model with fixed anisotropy. Open red circles represent data obtained from SdH measurements in fields only up to 14 T for $Pb_{1-x}Tl_xTe$; the f_{max} data point for the highest Na concentration is represented by a gray square in order to emphasize possible deviations from perfect ellipsoidicity seen in this sample; and the f_{max} data points for the two highest Tl concentrations (pink circles) were determined from f_{min} and assuming a constant pocket anisotropy $K = 14.3$ [15].

higher estimate of the carrier concentration than the L-pocket Luttinger volume for compositions above x_c. The near unchanging Luttinger volume indicates that E_F has become almost fixed at around 130 meV for $x > x_c$, in sharp contrast to $Pb_{1-x}Na_xTe$ [Fig. 4(b)]. E_F was calculated via Kane's model for an ellipsoidal nonparabolic band that has been shown to be appropriate for the L-pocket in PbTe [47,48]. The applicability of Kane's model further allows the

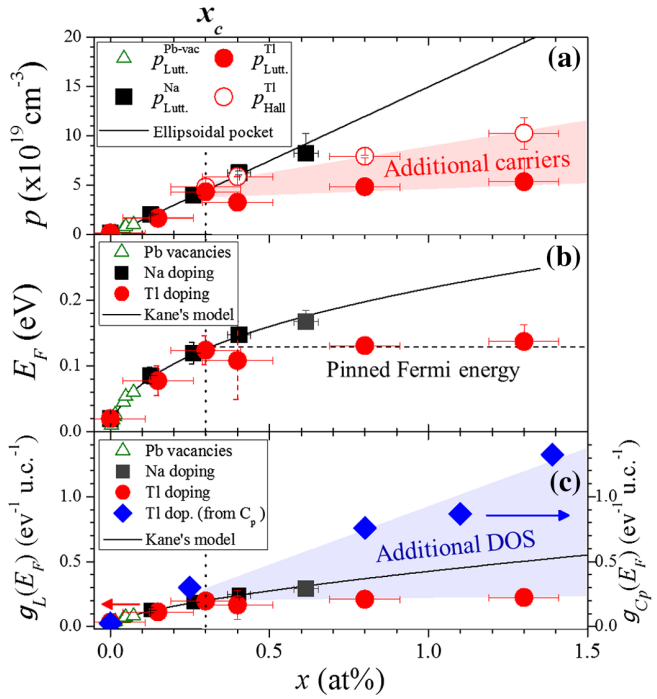

FIG. 4. (a) Evolution of the Luttinger volume of the L-pocket obtained from quantum oscillation measurements, (b) Fermi energy (E_F), measured from the valence band edge at the L-point, and (c) density of states at E_F [$g(E_F)$] as a function of dopant concentration, x. Data for self-doped PbTe ($p^{\text{Pb-vac}}_{\text{Lutt}}$.) shown by green-triangles, Na-doped PbTe ($p^{\text{Na}}_{\text{Lutt}}$) by black-squares, and Tl-doped PbTe ($p^{\text{Tl}}_{\text{Lutt}}$) by red-filled circles. Estimates of the carrier density obtained from p_H for Tl-doped samples ($p^{\text{Tl}}_{\text{Hall}}$) are shown by red-open circles in panel (a). In all three panels, the expected evolution of a single band ellipsoidal FS, assuming one hole per dopant and Kane's model, is shown by a black curve [47,51,52]. E_F and $g(E_F)$ as calculated from the experimentally determined L-pocket Luttinger volume and a single-band Kane's model dispersion [$g_L(E_F)$, left-axis]. Blue-diamonds in (c) represent the total DOS of Tl-doped PbTe samples as obtained from the electronic contribution to the heat capacity in Ref. [43] ($g_{Cp}(E_F)$, right-axis). Pink-shaded region in panel (a), and blue-shaded region in panel (c), indicate respectively the additional carriers and additional DOS found for Tl-doped PbTe that do not belong to the L-pockets.

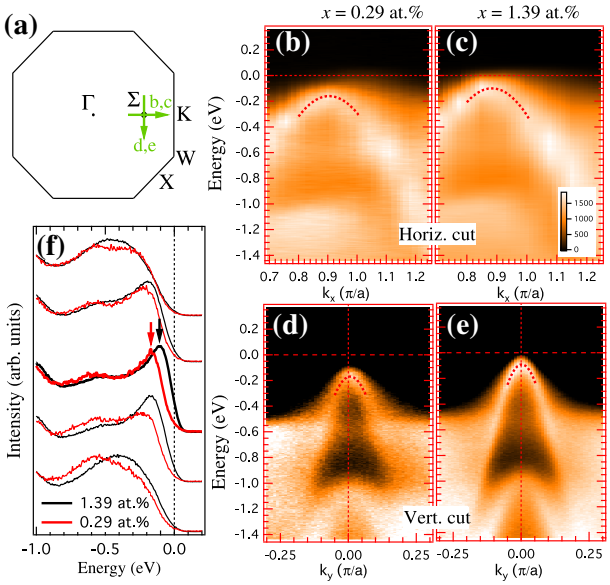

FIG. 5. Band structure analysis of the Σ-pocket for two different Tl concentrations illustrating that the Σ-pocket remains below E_F for all Tl compositions. Dotted curves are guides to the eye. (a) Projection of the Brillouin zone showing the momentum locations of band dispersion data (green arrows). (b)–(c) Band dispersion data of the Σ-band along the Γ-Σ direction, measured for Tl concentration (b) $x = 0.29\%$ and (c) $x = 1.39\%$. (d)–(e) are the same as (b)–(c) but along the direction perpendicular to the Γ-Σ direction. (f) Energy distribution curves at selected momentum points in vicinity of the Σ-pocket top, shown for both Tl dopings. Black and red arrows point the locations of the top of the Σ-band. The top of the Σ-pocket is found to lie well below E_F for all Tl concentrations.

electronic DOS of the L-pocket to be estimated and thus compared to the value derived from the Sommerfeld coefficient of the specific heat that necessarily encompasses all states at the Fermi energy. Similarly to the comparison between the Luttinger volume and the Hall effect, if all states are accounted for in the L-pocket, then these values should be in agreement, but Fig. 4(c) shows a large surplus [blue-shaded area, Fig. 4(c)] of DOS observed via heat capacity for $x > x_c$ in $Pb_{1-x}Tl_xTe$ that cannot be accounted for by the L-pocket observed in the present data. Whilst some of this anomalous increase in the DOS could be due to a zero-bias peak associated with the charge-kondo effect proposed in this material [42], when taken together with the discrepancy between the Luttinger volume and p_H [shaded area, Fig. 4(a)] it is natural to conclude that there must be additional mobile states outside of the L-pocket that continue to increase in number with increasing composition, despite E_F being almost constant [15].

Although the data shown in Figs. 3 and 4 confirm the presence of additional carriers outside of the L-pocket, they do not unambiguously differentiate between the resonant impurity state and Σ-pocket scenarios. The quantum oscillation amplitude is expected to be significantly smaller for the Σ-pocket, owing to its low mobility relative to the L-pocket [48], and therefore it could be present but unobserved in the data. Furthermore, the relatively large DOS expected for the Σ-pocket could give the impression that E_F is pinned, which is the expectation for an impurity state that is well defined in energy, as $(dE_F)/(dx)$ is significantly reduced as E_F reaches the Σ-band edge. To confirm that the Σ-pocket remains below E_F for $x > x_c$ in superconducting $Pb_{1-x}Tl_xTe$ low-temperature ARPES measurements were performed, the results of which are shown in Fig. 5. Figure 5(a) shows the location and direction in the k_x, k_y plane of the band dispersion data shown in Figs. 5(b)–5(e) for the main and transverse axes

of the Σ-pocket. The location of the Σ-point was determined from photon energy k_z scans. The Σ-band at this point is weakly k_z dispersive. In both compositions measured, $x = 0.29\% \approx x_c$ [Figs. 5(b) and 5(d)] and $x = 1.39\% > x_c$ [Figs. 5(c) and 5(e)], the Σ-band is seen to remain below E_F by approximately 170 meV and 100 meV, respectively. This is consistent with existing ARPES results that also conclude that only the L-pocket crosses E_F for a sample of $x = 0.5\%$ [53]. This result strongly supports the conclusion that the Σ-pocket is not responsible for the anomalous Fermiology and superconductivity in $Pb_{1-x}Tl_xTe$ at $x > x_c$.

The experimental results presented here lead to a number of robust conclusions about the nature of the Fermiology of $Pb_{1-x}Tl_xTe$. The key conclusion is that the Σ-pocket remains well below E_F for all of the compositions measured, directly showing that this additional band maximum is not responsible for superconductivity. Moreover, E_F becomes pinned in a narrow band of energies for $x > x_c$, coincidentally with the onset of superconductivity, which has previously been inferred but never definitively established [13,14,42,54]. Also, despite E_F being pinned, we find evidence that additional mobile carriers are present but not associated with a coherent FS pocket, which could not previously have been inferred from existing data [55]. All of these conclusions strongly support the impurity band scenario illustrated in Fig. 1(b), and they are inconsistent with the Σ-pocket scenario shown in Fig. 1(a). This study provides the strongest experimental evidence to date that attention should be focused on the Tl impurity states in order to understand the superconductivity of Tl-doped PbTe.

It remains to be seen how the resonant impurity states contribute to the enhanced superconductivity in Tl-doped PbTe. Existing data in very heavily doped $Pb_{1-x}Na_xTe$ achieves a similar DOS to that seen in superconducting $Pb_{1-x}Tl_xTe$, yet it still does not exhibit superconductivity down to 10 mK, which directly implies that it is the pairing interaction ($V_{kk'}$ from the BCS gap equation) that is introduced extrinsically by the Tl dopants [56] that is the key factor determining the onset of superconductivity. Phenomenological models that capture the elements of the electronic structure associated with these impurities certainly indicate that charge fluctuations can provide an effective pairing interaction [39,44]. It is also possible that the impurity states locally induce an enhanced e-ph interaction, possibly due to correlation effects, similar to what has been proposed for doped $BaBiO_3$ [57]. Independently of these questions, the understanding of the evolution of the electronic structure of $Pb_{1-x}Tl_xTe$ points the way towards the design of other superconductors based on a similar mechanism.

We thank Y. Matsushita and A. S. Erickson for the crystal growth of some of the samples used in this study, T. Geballe, M. Fechner, and P. V. C. Medeiros for insightful discussions, and C. Bell for insights that have improved the manuscript. P. G. G., P. W., and I. R. F., and work performed at Stanford University, were supported by AFOSR Grant No. FA9550-09-1-0583. B. S. and N. A. S. acknowledge support from ETH Zürich, the ERC Advanced Grant program (No. 291151), and the Swiss National Supercomputing Centre (CSCS) under Project IDs s307, s624, and p504. The high-field magnetoresistance measurements were performed at the National High Magnetic Field Laboratory (NHMFL), which is supported by NSF DMR-1157490, the State of Florida (DC facility), and the DOE/BES Science at 100T grant (pulsed field facility); and the High Field Magnet Laboratory, Radboud University/Fundamental Research on Matter, member of the European Magnetic Field Laboratory and supported by EuroMagNET II under European Union (EU) Contract No. 228043. Work at Ames Laboratory (ARPES measurements) was supported by the U.S. Department of Energy, Office of Basic Energy Sciences, Division of Materials Sciences and Engineering. Ames Laboratory is operated for the U.S. Department of Energy by the Iowa State University under Contract No. DE-AC02-07CH11358. The Advanced Light Source is supported by the Director, Office of Science, and Office of Basic Energy Sciences of the U.S. Department of Energy under Contract No. DE-AC02-05CH11231.

[1] K. Ueno, S. Nakamura, H. Shimotani, H. T. Yuan, N. Kimura, T. Nojima, H. Aoki, Y. Iwasa, and M. Kawasaki, Nat. Nanotechnol. **6**, 408 (2011).
[2] E. Bustarret, Physica (Amsterdam) **514C**, 36 (2015).
[3] L. P. Gor'kov, Phys. Rev. B **93**, 054517 (2016).
[4] L. P. Gor'kov, Proc. Natl. Acad. Sci. U.S.A. **113**, 4646 (2016).
[5] Y. Takada, J. Phys. Soc. Jpn. **49**, 1267 (1980).
[6] J. Appel, Phys. Rev. **180**, 508 (1969).
[7] J. M. Edge, Y. Kedem, U. Aschauer, N. A. Spaldin, and A. V. Balatsky, Phys. Rev. Lett. **115**, 247002 (2015).
[8] X. Lin, G. Bridoux, A. Gourgout, G. Seyfarth, S. Krämer, M. Nardone, B. Fauqué, and K. Behnia, Phys. Rev. Lett. **112**, 207002 (2014).
[9] G. Binnig, A. Baratoff, H. E. Hoenig, and J. G. Bednorz, Phys. Rev. Lett. **45**, 1352 (1980).
[10] R. M. Fernandes, J. T. Haraldsen, P. Wolfle, and A. V. Balatsky, Phys. Rev. B **87**, 014510 (2013).
[11] M. L. Cohen, Phys. Rev. **134**, A511 (1964).
[12] O. Prakash, A. Kumar, A. Thamizhavel, and S. Ramakrishnan, Science **355**, 52 (2017).
[13] S. A. Nemov and Y. I. Ravich, Sov. Phys. Usp. **41**, 735 (1998).
[14] V. I. Kaidanov and Y. I. Ravich, Sov. Phys. Usp. **28**, 31 (1985).
[15] See Supplemental Material at http://link.aps.org/supplemental/10.1103/PhysRevLett.121.207001 for DFT band structure calculations (which includes Refs. [16–30]), crystal growth details (which includes Ref. [31]), full magnetoresistance data sets, analysis of Fermi surface parameters, high-field Hall data, and effective cyclotron mass determination (which includes Refs. [32–36]).

[16] P. E. Blöchl, Phys. Rev. B **50**, 17953 (1994).
[17] G. Kresse and D. Joubert, Phys. Rev. B **59**, 1758 (1999).
[18] G. Kresse and J. Furthmüller, Phys. Rev. B **54**, 11169 (1996).
[19] J. P. Perdew, A. Ruzsinszky, G. I. Csonka, O. A. Vydrov, G. E. Scuseria, L. A. Constantin, X. Zhou, and K. Burke, Phys. Rev. Lett. **100**, 136406 (2008).
[20] E. S. Božin, C. D. Malliakas, P. Souvatzis, T. Proffen, N. a. Spaldin, M. G. Kanatzidis, and S. J. L. Billinge, Science **330**, 1660 (2010).
[21] P. V. C. Medeiros, S. Stafström, and J. Björk, Phys. Rev. B **89**, 041407(R) (2014).
[22] P. V. C. Medeiros, S. S. Tsirkin, S. Stafström, and J. Björk, Phys. Rev. B **91**, 041116(R) (2015).
[23] L.-W. Wang, L. Bellaiche, S.-H. Wei, and A. Zunger, Phys. Rev. Lett. **80**, 4725 (1998).
[24] V. Popescu and A. Zunger, Phys. Rev. Lett. **104**, 236403 (2010).
[25] V. Popescu and A. Zunger, Phys. Rev. B **85**, 085201 (2012).
[26] B. Sangiorgio, Ph.D. thesis, ETH Zurich, 2017.
[27] W. Ku, T. Berlijn, and C.-C. Lee, Phys. Rev. Lett. **104**, 216401 (2010).
[28] P. B. Allen, T. Berlijn, D. A. Casavant, and J. M. Soler, Phys. Rev. B **87**, 085322 (2013).
[29] S. Ahmad, K. Hoang, and S. D. Mahanti, Phys. Rev. Lett. **96**, 056403 (2006).
[30] K. Hoang and S. D. Mahanti, Phys. Rev. B **78**, 085111 (2008).
[31] Y. Matsushita, Ph.D. thesis, Stanford University, 2007.
[32] M. M. Altarawneh, C. H. Mielke, and J. S. Brooks, Rev. Sci. Instrum. **80**, 066104 (2009).
[33] E. A. Yelland, J. Singleton, C. H. Mielke, N. Harrison, F. F. Balakirev, B. Dabrowski, and J. R. Cooper, Phys. Rev. Lett. **100**, 047003 (2008).
[34] D. Shoenberg, *Magnetic Oscillations in Metals* (Cambridge University Press, Cambridge, England, 1984).
[35] Y. Nagaoka, Phys. Rev. **138**, A1112 (1965).
[36] H. Suhl, Phys. Rev. **138**, A515 (1965).
[37] S. Ahmad, S. D. Mahanti, K. Hoang, and M. G. Kanatzidis, Phys. Rev. B **74**, 155205 (2006).
[38] K. Xiong, G. Lee, R. P. Gupta, W. Wang, B. E. Gnade, and K. Cho, J. Phys. D **43**, 405403 (2010).
[39] M. Dzero and J. Schmalian, Phys. Rev. Lett. **94**, 157003 (2005).
[40] H. Matsuura and K. Miyake, J. Phys. Soc. Jpn. **81**, 113705 (2012).
[41] T. A. Costi and V. Zlatić, Phys. Rev. Lett. **108**, 036402 (2012).
[42] Y. Matsushita, H. Bluhm, T. H. Geballe, and I. R. Fisher, Phys. Rev. Lett. **94**, 157002 (2005).
[43] Y. Matsushita, P. A. Wianecki, A. T. Sommer, T. H. Geballe, and I. R. Fisher, Phys. Rev. B **74**, 134512 (2006).
[44] C. M. Varma, Phys. Rev. Lett. **61**, 2713 (1988).
[45] A. Taraphder, Rahul Pandit, H. R. Krishnamurthy, and T. V. Ramakrishnan, Int. J. Mod. Phys. B **10**, 863 (1996).
[46] A. W. Sleight, Physica (Amsterdam) **514C**, 152 (2015).
[47] P. Giraldo-Gallo, B. Sangiorgio, P. Walmsley, H. J. Silverstein, M. Fechner, S. C. Riggs, T. H. Geballe, N. A. Spaldin, and I. R. Fisher, Phys. Rev. B **94**, 195141 (2016).
[48] Y. I. Ravich, *Semiconducting Lead Chalcogenides* (Springer, New York, 1970).
[49] J. D. Jensen, B. Houston, and J. R. Burke, Phys. Rev. B **18**, 5567 (1978).
[50] J. R. Burke, B. Houston, and H. T. Savage, Phys. Rev. B **2**, 1977 (1970).
[51] E. O. Kane, J. Phys. Chem. Solids **1**, 249 (1957).
[52] E. O. Kane, *Semiconductors and Semimetals* (Academic, New York, 1975), Vol. 1.
[53] K. Nakayama, T. Sato, T. Takahashi, and H. Murakami, Phys. Rev. Lett. **100**, 227004 (2008).
[54] J. P. Heremans, V. Jovovic, E. S. Toberer, A. Saramat, K. Kurosaki, A. Charoenphakdee, S. Yamanaka, and G. J. Snyder, Science **321**, 554 (2008).
[55] The absence of the impurity band in our ARPES measurements is explained by unfolding our DFT calculations of Tl-doped PbTe supercells (see SM), which show that the band has low spectral weight.
[56] I. Chernik and S. Lykov, Tverd. Tela **23**, 2956 (1981) [Sov. Phys. Solid State **23**, 1724 (1981).]
[57] Z. P. Yin, A. Kutepov, and G. Kotliar, Phys. Rev. X **3**, 021011 (2013).